Title: Residual Stress Measurement of Full-Scale Jet-Engine Bearing Elements Using the Contour Method

Author(s): Prime, Michael Bruce
Isaac, Daulton Duggart
Arakere, Nagaraj K

Intended for: XIII International Congress and Exposition on Experimental and Applied Mechanics, 2016-06-06/2016-06-09 (Orlando, Florida, United States)

Issued: 2016-02-26

Isaac DD, Prime MB, Arakere N (2016) Residual Stress Measurement of Full-Scale Jet-Engine Bearing Elements Using the Contour Method. Quinn S, Balandraud X (eds) Residual Stress, Thermomechanics & Infrared Imaging, Hybrid Techniques and Inverse Problems, Volume 9: Proceedings of the 2016 Annual Conference on Experimental and Applied Mechanics. Springer International Publishing, pp 69-81. doi:10.1007/978-3-319-42255-8_10

Residual Stress Measurement of Full-Scale Jet-Engine Bearing Elements Using the Contour Method

Daulton D. Isaac[1, 2], Michael B. Prime[2], Nagaraj Arakere[1]
1. University of Florida, Department of Mechanical and Aerospace Engineering, Gainesville, FL USA.
2. Los Alamos National Laboratory, Los Alamos, NM USA.

ABSTRACT

Compressive residual stresses provide a well-known advantage to the fatigue life of bearing materials under rolling contact fatigue (RCF), but the stresses change under fatigue loading and may later contribute to failures. Previous measurements of the depth-wise distribution of residual stresses in post-fatigue bearings with X-rays involved the time consuming process of etching to determine subsurface stresses and only in limited locations. By contrast, the contour method determines the 2D residual stress map over a full cross section. The method involves the sectioning of the part using Electrical Discharge Machining, measuring the out of plane displacements of the exposed cross section, and using the afforded field as boundary conditions on a finite element model of the component to back calculate the causative residual stress. For this investigation, the residual hoop stresses in the split inner rings of the main shaft bearing assembly of an aircraft jet engine was mapped using the contour method. Prior to measurement, the full-scale bearing made of hardened AISI M50 was subjected to RCF during engine operation. In this talk, the unique challenges of the particular measurements are discussed. The tested bearings showed effectively no residual stresses induced by the RCF, probably because they were conservatively removed from service prior to sufficient cyclic loading. More highly loaded bearing will be measured in future work.

Keywords: rolling contact fatigue, bearings, contour method, residual stress, finite element model

INTRODUCTION

Residual stresses play a significant role in many material failure processes like fatigue, fracture, fretting fatigue, and stress corrosion cracking [1-3]. Residual stresses are the stresses present in a part free from external load, and they are generated by virtually any manufacturing process. Because of their important contribution to failure and their almost universal presence, knowledge of residual stress is crucial for prediction of the life of any engineering structure. However, the prediction of residual stresses is a very complex problem. In fact, the development of residual stress generally involves nonlinear material behavior, phase transformation, coupled mechanical and thermal problems and also heterogeneous mechanical properties [4-20].

Residual Stresses and Roller Bearings

In this subsection, we make the points that residual stresses in general, and the radial component of residual stress in particular, 1) are important in the fatigue life of roller bearings, 2) are usually ignored, and 3) are difficult to measure.

Bearing steels are a family of ultra-high-strength structural materials subjected to the highest loading conditions in engineering systems throughout their life cycle. Some grades have tensile strengths exceeding 2.7 GPa and hardness values beyond 900 HV (~9 GPa). Industries have been aggressively pursuing development of new bearing steels to meet the increasingly challenging requirements for high power density, operation under transient adverse conditions and reliability of bearings for applications accumulating over 100 billion (10^{11}) cycles in aircraft, wind turbine, high-speed railway and other systems. The requirement for the L10 life, defined as the number of cycles at which 90% of bearings survive under a rated load and speed, can be in excess of 30,000 hours, about 100 billion (10^{11}) cycles of contacts. Properly installed and maintained bearings eventually fail under the influence of Rolling Contact Fatigue

(RCF). RCF manifests as highly localized damage, accumulated under the contact surface, typically at a depth of 200-400 μm, eventually leading to the nucleation of subsurface cracks. Carbide precipitates ranging from tens of nm to 1-5 μm are largely responsible for material hardening.

Bearing material is subjected to a radically different fatigue loading under RCF compared to conventional high cycle fatigue (HCF). The salient features of RCF are:

(i) The volume of cyclically stressed subsurface material in the RCF-affected zone is only a few $mm^3$and highly localized [21].
(ii) Nature of cyclic fatigue loading is triaxial and nonproportional, over a very large number of cycles (~10^{11}). The ability of material to work harden is much greater under these conditions.
(iii) Although loading is nominally elastic, heterogeneous cyclic plasticity at the scale of microstructure (i.e., microplasticity) is induced [22-24].
(iv) Material microstructure, residual stress and micro-hardness in the RCF-affected zone evolve continuously with cycles, with progressive fatigue damage accumulation [21,22]. Tensile residual stresses in the radial direction are known to develop that can drive Mode I subsurface crack growth parallel to the running surface.

Bearing fatigue life estimation is still largely based on the seminal probabilistic life model by Lundberg and Palmgren (LP) [25-27], proposed in 1945. Despite many improvements to the LP model [21] current bearing life prediction methods are based on the ISO standard [28] and continue to rely on extensions to the LP model, are empirical in nature, and include variables that are obtained from extensive experimental testing. They do not directly consider the subsurface residual stress evolution, details of the constitutive behavior of materials under contact loading or localized microplasticity. Generally, LP models significantly underpredict bearing life.

Bearing life, based on LP models, can expressed as [25]

$$L \propto \frac{1}{[F_e]^p} \propto \frac{1}{S^n} \quad (1)$$

Where, $L, F_e, and\ S$ represent bearing fatigue life, equivalent radial load, and maximum Hertzian contact pressure, respectively. In Eq. 1, p and n are the load-life and stress-life exponents respectively. Based on LP models, stress-life exponent is 9 for ball bearings. The reevaluation study by Parker and Zaretsky [29] indicates that load-life exponent and stress-life exponent for vacuum-processed steels are 4 and 12 respectively. However, a recent study [30] has shown that the load life exponent for ball bearings should be 4.1 (instead of 3 or 4), and the corresponding stress-life exponent should be 12.3. This shows that bearing life is highly sensitive to the small changes in the subsurface Hertzian stress due to the large exponent value of 12.

Peak Hertzian contact stresses in aerospace bearings are typically 2.0-2.5 GPa (290-370 ksi) [21]. The peak orthogonal shear stress for this condition is about 600 MPa. The residual stress development is primarily the result of the accommodation of shape change of the small volume of RCF-induced plastic zone upon loading. SAE 52100 steel ball bearings (10-15% retained austenite) tested at peak Hertzian stress of 3.3 GPa (485 ksi) developed a maximum compressive circumferential residual stress of 900 MPa after 2×10^9 inner ring revolutions, ~250 μm below the surface [31]. Axial compressive residual stresses were of similar magnitude while radial *tensile* residual stress of about 300 MPa persisted to greater depths of ~1.5 mm in the radial normal direction [31]. This indicates that the residual stresses developed in long-life bearings can be substantial, resulting in a perturbation of the Hertzian contact stress field, leading to significant variability in life prediction via Eq. (1).

The presence of subsurface residual stresses in bearings will certainly influence life calculations from Eq. (1). However, residual stress measurement [32] in bearing raceways is not easy and they evolve with RCF cycles. The important stresses are generally localized within a few 100 micrometers of the surface, which makes bulk measurement methods like neutron diffraction [33] impractical. Conventional hole drilling [34] is not possible because the steels are too hard to drill. X-ray diffraction has been used to

measure residual stresses in bearings [31], but requires material removal to get subsurface stresses and typically only measures the circumferential residual stress. Hence, residual stresses are not adequately accounted for in life calculations. Compressive residual stresses that exist in case hardened bearings from manufacturing processing are known to greatly enhance life.

The influence and role of residual stress in the operation and life of RCF components being thus highlighted, it is understandable that such a parameter needs to be more fully understood. This paper presents a comprehensive method for residual stress measurement in rolling element bearings.

Bearing Residual Stress Measurements with the Contour Method

In this subsection, we describe how the residual radial stresses could be measured using a combination of the contour method with x-ray diffraction using superposition [35]. In this paper, only the results from the initial contour method measurements are reported.

The Contour Method [36] is a relatively new technique for measuring residual stresses [37,38] but well proven and validated [39-48]. Figure 1 illustrates the ideas behind the technique. Step A in the figure represents a part containing residual normal stresses σ_x and σ_z that vary over the height of the beam. If the part is cut, the surface exposed will deform elastically owing to the relaxation of the residual stresses as shown in Step B. Notice that σ_x must fully relax because it is normal to the newly created free surface. Because the deformation was elastic, forcing the deformed face back flat would reintroduce the stresses back into the part. Thus, if the deformations are measured and their reverse are applied as displacements on the surface of an unstressed part of similar geometry (as the deformed part) , the residual stresses that relaxed during the initial deformation will be induced in this part as shown in Step C of the figure. In the contour method, a part containing residual stress is sectioned allowing the stresses to deform the exposed face. The out of plane displacement of this surface is then measured, for example with a coordinate measuring machine. In a linear elastic finite element analysis on the sectioned part, the opposite of the obtained contour is applied to an unstressed model of the part, and the resulting stresses are the stresses that changed as a result of the relaxation caused by the sectioning, i.e. C = A - B. Since the normal stress σ_x is zero in the free surface in B, this calculation gives the original (A) 2-D residual σ_x distribution on the full cross-section of the cut plane.

In order to get the radial stress, a hybrid variation of the contour method [35] is of particular interest for the case of RCF in bearings. The most logical cut to make when applying the method to a bearing race is one that exposes a radial-axial cross section (see Figure 2). The residual hoop stresses act normal to that section and thus is the only component that can be fully obtained through the standard contour method. Referring back to Figure 1, we consider in particular the right side of the figure which depicts the behavior of the in-plane normal stress σ_z, which is analogous to the radial stress for our bearing measurements. Upon sectioning, the distribution of σ_z indeed changes as shown in Step B, but it is not fully relaxed. The amount that σ_z relaxed is actually quantifiable through the same operation of pushing back flat the deformed face as can be seen in Step C. This shows that although the contour method can only fully determine the stress component acting normal to the exposed surface, it can also determine the partial relaxation of normal stresses acting in the plane of the surface. In the case of a bearing, exposing the radial axial cross section allows for full determination of the residual hoop stresses and for quantifying how much the radial and axial components relaxed due to sectioning. Using a residual stress measurement technique that can measure in-plane stresses, such as X-Ray Diffraction, the unrelaxed portion of stress can be measured and combined with the relaxed portion to fully determine the in-plane normal stresses present in the bearing ring before sectioning. This is of particular interest seeing the residual radial stress in bearings, thought to be tensile, may play a role in Mode I crack growth. This new multiple-method superposition technique with the contour method [35], has been demonstrated a few times in the literature [49,40,50].

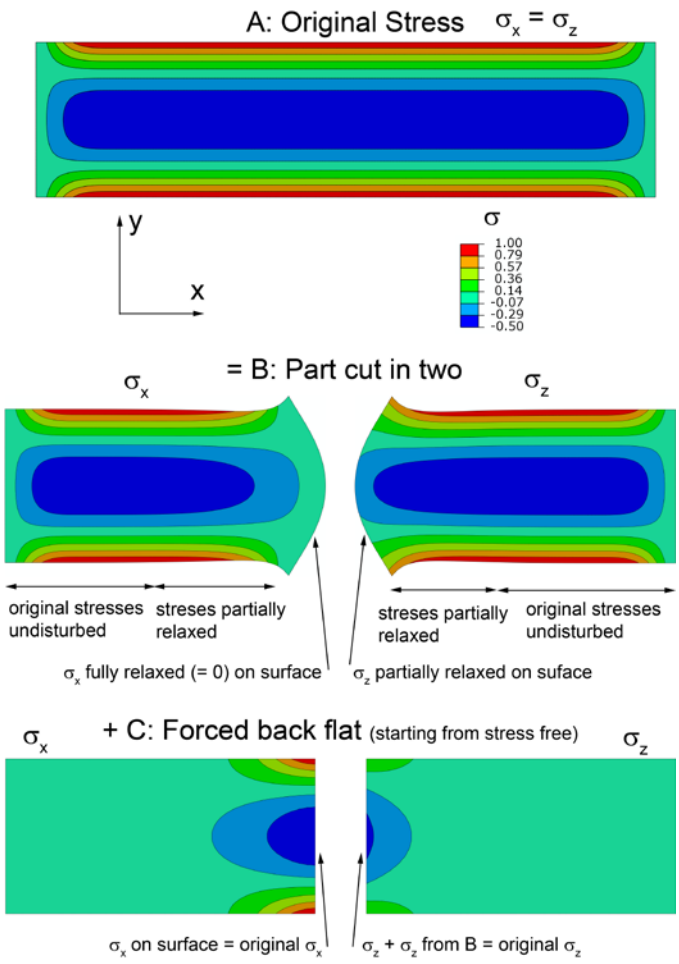

Figure 1 Superposition Principle Behind the Contour Method

Special attention has to be paid when utilizing the Contour Method to measure hoop stresses in cylindrical bodies such as pipes or as in this case a bearing ring [51,49,52-54]. Assuming axisymmetry, the residual stresses on each cross section along the circumference of such geometries would be in force equilibrium, but there can be a net bending moment acting to either open up or close the part. Cutting through a section with a bending moment can result in a large load on the cut tip and local yielding [51,53,55], which clearly violates the elastic deformation assumption of the method. To reduce or eliminate plasticity, this bending residual stress is first relieved by cutting open the cylindrical part, and the contour method measurement is then made at another section on the circumference. However, the bending stresses relieved are of interest since they act in concert with the force equilibrium stresses to produce the net residual stress field, so measures are taken to calculate these stresses [51,54] as discussed later in the paper.

Purpose

The work reported seeks to make a novel application of the contour method to determine the distribution of the residual stress present in the rings of a through hardened inner bearing race. Ideal cutting parameters, profiling techniques, data processing steps, and finite element modeling methods are sought after in an attempt to uncover the contour method particulars best adapted to measurement in bearings. Thus insight is offered on the state of residual stress in a bearing taken out of operation and on best practices to enable and continue a broad study of the phenomenon in high performance bearings using the contour method.

Methods

Experimental

The inner bearing rings under investigation are from the main shaft bearing assembly taken out of operation in an airplane jet engine. The bearing as shown in Figure 2 is of the split inner ring type, and has a bore diameter of about 133 mm and an outer diameter of 200 mm. The through hardened M-50 bearing steel typically has a uniform carbon content of 0.85 wt.% throughout its depth with a carbide volume fraction of 20%. The primary carbides range in size from 1-5 μm. This high strength bearing steel has a hardness of about 8 GPa (63-65 HRC) with an yield strength of 2.8 GPa.

No spalls or other defects were observed on either of the rings taken from service. The stress level and cycles experienced by the bearing is unknown. Since this is a thrust bearing, one inner ring bears significantly more of the load. As such, the bearings are referred to as the thrust-loaded and unloaded bearings and their cross-sectional geometries are differentiable. The work described below is applicable to both rings. However, the contour data was processed into a residual map only for the unloaded race for reasons addressed in the Results and Discussion section.

Particulars of the cut plan and reasoning.

In order to determine the residual hoop stresses present, a cut in the radial-axial plane, shown in Figure 2, into the bearing is required. Figure 3 illustrates the location of the various cuts made into the rings of the inner race. In general, the operations carried out on the two rings were similar. First the stress release cut is made, which results in the relieving of the bending moment stresses present in the ring. A strain gage is used at the location shown to capture the strain from the ring springing open when sectioned. The strain value is used in a finite element model of each ring to determine the bending residual stresses that were relieved. 180 degrees from the location of the stress release cut, the contour cut is performed after the strain gage is removed. The out of plane displacement of the newly exposed surfaces of this cut is later used for determining the force equilibrium residual stresses. The measured displacement data from both sides of the cut is aligned on a common grid before being averaged. The averaging of the data from both sides removes the effects of cutting artifacts and shear stresses.

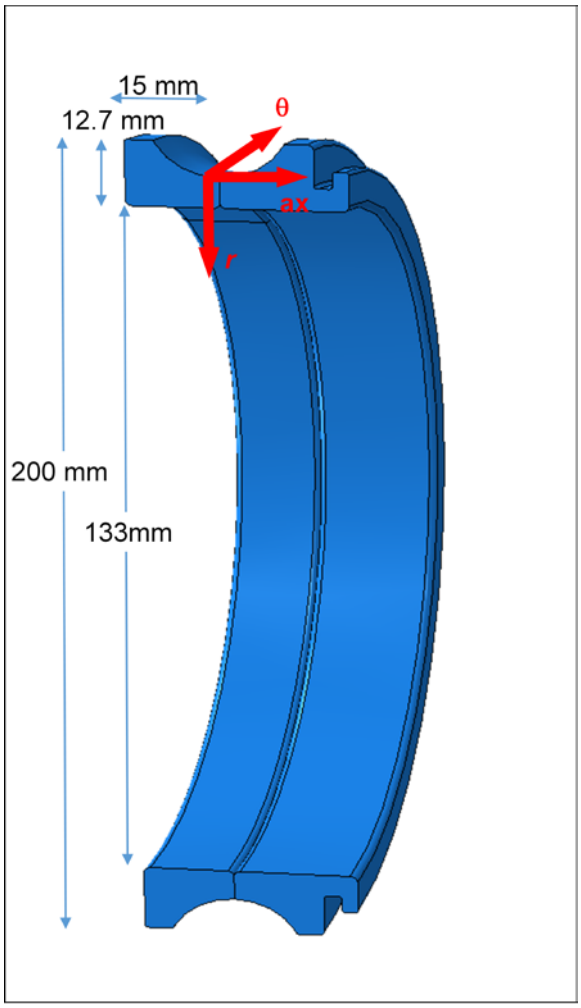

Figure 2 Showing basic dimensions of the bearing and the radial-axial cross section with the three components of residual stress

To remove the effects of noisy data, the averaged data is fitted to a smooth 3D surface using cubic splines, and the best fit is evaluated on the basis of a least squares analysis. The fitted surface is then evaluated at coordinates corresponding to the nodes of the finite element mesh of the ring model, and the analysis continues as discussed in the Finite Element Modeling section below.

The third and final cut is the stress-free test cut [36,56,57,52] and is made by slicing a thin wafer off of one of the faces exposed by the stress release cut. The stress free cut should result in a flat surface seeing that the normal residual stresses were already released by the stress release cut. Any displacement measured from this last cut can be regarded as connected to the cutting of the part, and they can be used to make corrections to the displacement from the contour cut.

A 100 μm wire was used to perform the contour and stress free cuts using the skim cutting setting. The normal displacements of the contour faces were measured using a Taylor Hobson Talyscan 250 with a laser triangulation probe, and a grid of 50 X 50 μm was used to map the contour of the surface.

Finite Element Modeling

The value for the average strain obtained from the bending-moment stress release cut can be used to scale a model of each ring to determine the bending stresses that caused the ring to deform at this cut.

The average strain at the location corresponding to that of the strain gage in the actual ring could then be calculated. The deformation being linear, the forces in the model can be scaled until the strain in the model matches that obtained during the stress release cut. The bending stresses thus determined can later be superimposed with those determined through the surface profiling of the contour cut.

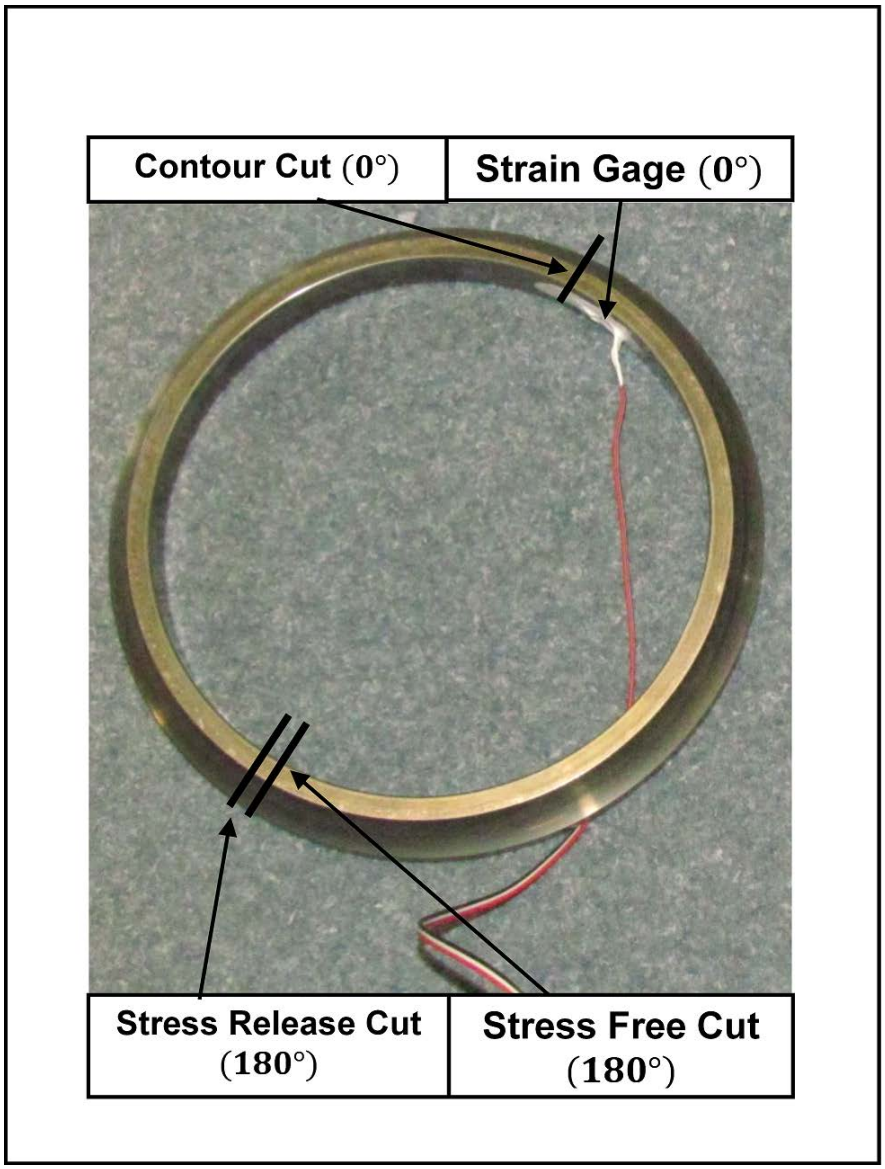

Figure 3 Various cuts made into the bearing. Cut 1 releases the geometric stresses, Cut 2 reveals the surface whose contour will be measured, and Cut 3 serves to check the validity of the surface obtained in the contour cut (Cut 2).

A 180 degree portion model with the deformations from the contour cut applied as boundary conditions is used to obtain the remaining residual stresses. The displacement boundary conditions are generated for the normal direction only. All other degree of freedoms are left unconstrained on the model, except for those necessary to prevent rigid body translation or rotation of the model.

Results and Discussion

Strains from the Bending Moment Release Cut

During the stress release cut, a value of -42 με was recorded by the strain gage for the thrust-loaded race, and -15 με for the unloaded race. The magnitude of the bending moment stresses is estimated at under 7 MPa, small enough to be ignored in the remainder of the calculations.

Results for the Measured Contours

The raw data indicates that the residual stresses in the bearing races are quite small and that the in-service loading did not induce any significant stresses. Figure 4 and Figure 5 show the measured contours for the thrust-loaded and unloaded bearing races, respectively. As is standard [36], the data is plotted relative to the best fit plane. The data all falls within ±10 μm, not much greater than the noise level of the data, indicating relatively small deformations caused by residual stress release. There are some high and low features in the contours that appear linear. These are all oriented in the wire direction and are almost certainly EDM-cutting artifacts [57]. At first glance, there appears to be a high spot near the surface of the curved bearing surface which might indicate some local stresses. For two reasons, further consideration indicates that such stresses are not evident or likely. First, the high spot appears in both the thrust-loaded race and the unloaded race at similar magnitudes, which would not be the case if the loading caused residual stresses. Second, the stress-free test cuts, Figure 6, show very similar high regions, further indicating that the feature is an EDM-cutting artifact. When an EDM wire cuts through a non-uniform cross-section, there are small deviations from a perfectly constant width cut, which show up as such artifacts [52]. The stress-free test cuts also show linear features, confirming that the similar features in Figure 4 and Figure 5 are cutting artifacts. In fact, the test cut for the thrust-loaded race, Figure 6a, shows larger features than the measurement data in Figure 4, which only indicates that there might have been some problem with the test cut. In all, the lack of significant differences between the measurement cuts and the stress-free test cuts indicate a lack of significant residual stresses.

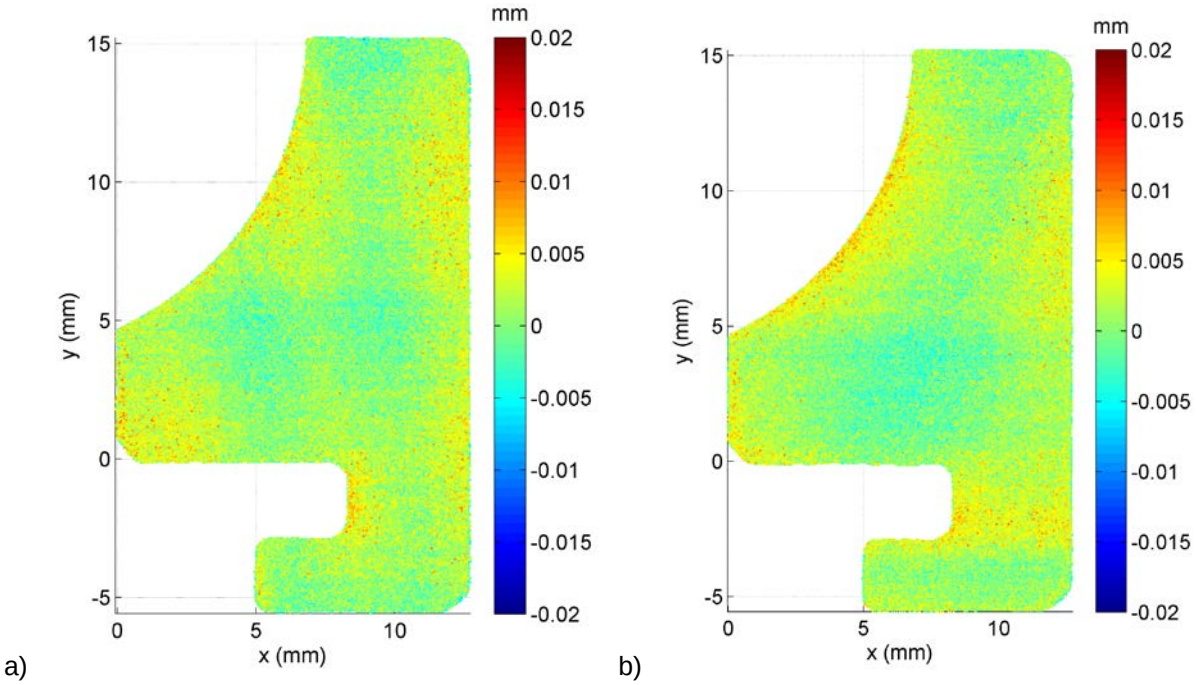

Figure 4. The surface height maps for the two halves of the thrust-loaded race show relatively small deformations.

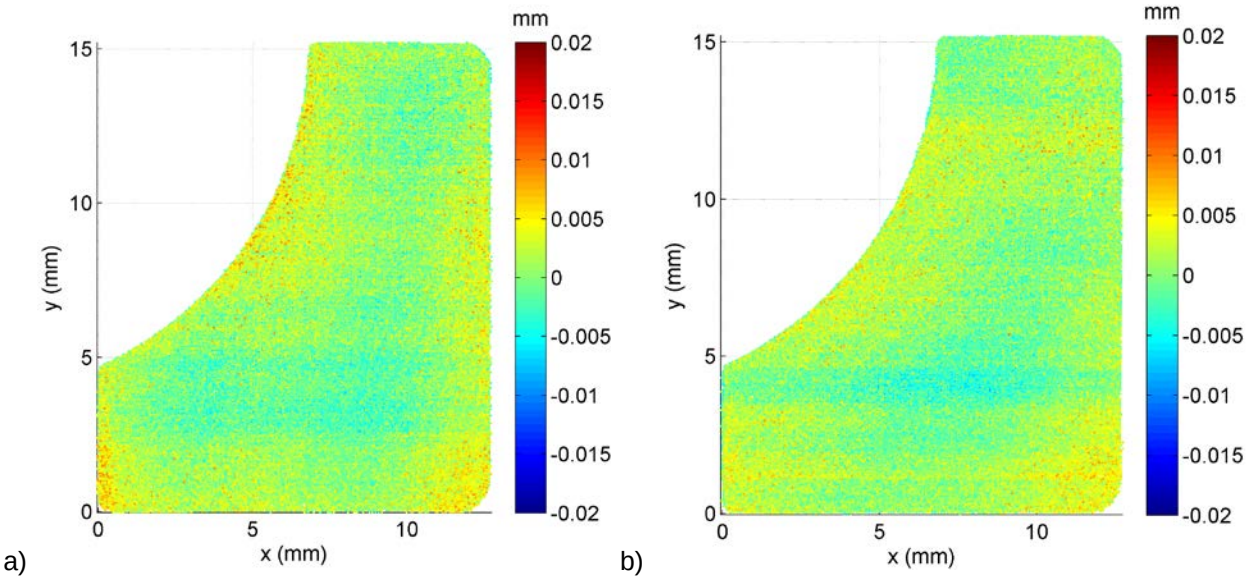

Figure 5. Surface height maps for the two halves of the unloaded race show similar features to the loaded race.

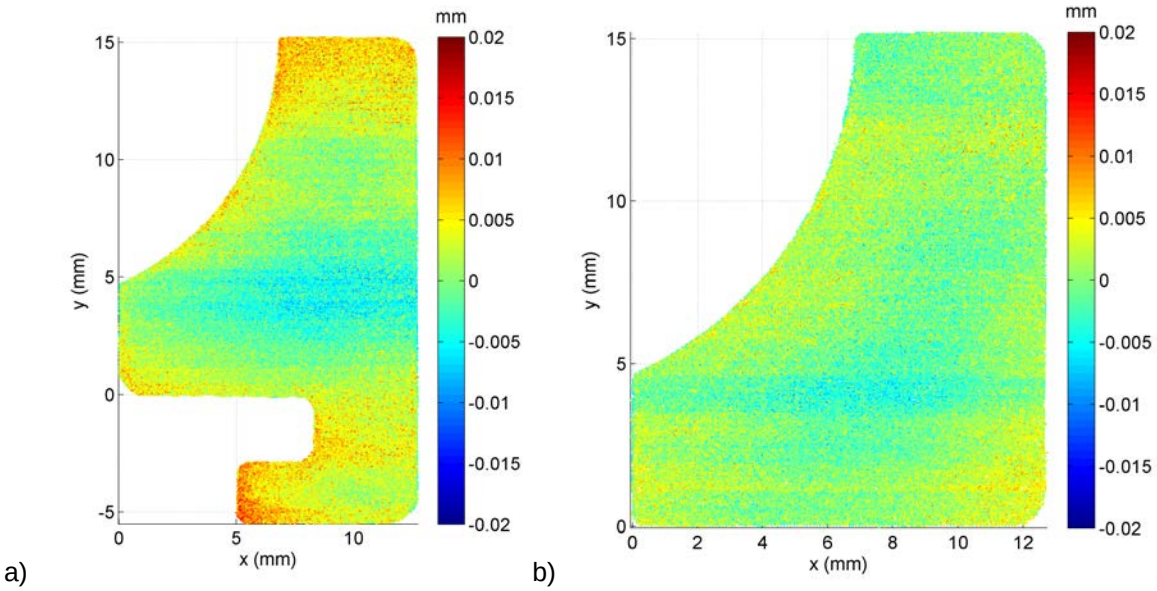

Figure 6. Surface height maps for the stress-free test cut for the a) loaded and b) unloaded races show similar deformation magnitudes to the measurements in Figure 5 and Figure 6.

The raw data should not be taken to indicate a significant deficiency in the contour method itself. Had significant stresses been induced by the in-service loading of the bearing, the measurement cuts would have given much larger contours than those in Figure 4 and Figure 5, and would have been large compared to the test cuts.

Because the unloaded race seemed to have the most representative stress-free test cut, that data was analyzed first. Following standard procedure [36,58], the measured contours, Figure 5, were interpolated onto a regular grid and then averaged point-by-point. The test cut, Figure 6b, was then interpolated onto the same grid. The test cut data was then subtracted from the averaged contour to reveal the deformations caused by residual stress relaxation [38,57,36,56]. The resulting contour shown in **Figure 7**

shows very little evidence of residual stress. There is no significant shape near the curved bearing surface. Linear horizontal features, indicative of small EDM cutting artifacts, remain because they are not exactly duplicated in the test cut so are not corrected out. Some slightly low regions in the lower left and upper right regions of the figure might indicated tensile residual stress regions that are balanced by compressive stresses in the lower right, but the features may not be experimentally significant.

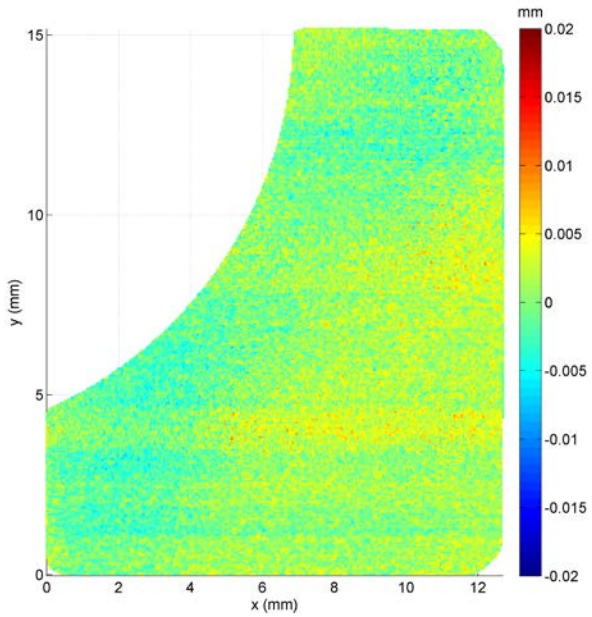

Figure 7. After being averaged between the two sides then corrected for the stress-free test cut, the measured contours from the unloaded race show little evidence of residual stress.

Residual Stresses

As expected from the data, no significant stresses are observed in the unloaded bearing race. When the deformations from **Figure 7** are processed into boundary conditions and applied to an unstressed model, the results are shown in Figure 8 are obtained. The stress uncertainty is estimated [58,59], to be at least ±50 MPa. The stresses are not plotted within 300 μm of the edges because of inherent contour-method limitations getting stresses close to edges [36]. The results show some indication of subsurface tensile stress regions that might arise from the hardening and other thermal processing of the parts. However, the stresses lack significance in two ways. First, the peak stresses are barely larger than the predicted uncertainties, and it is difficult to account for all uncertainties so they may be lower than the actual uncertainties. Second, and more important, such stress magnitudes are not significant for the fatigue behavior of the races.

Surface or case hardening often leads to very high residual stresses because of non-uniform plastic deformation and/or phase changes [11,60]. Because these races are through-hardened, the thermo-mechanical history is sufficiently uniform that significant residual stresses do not seem to be induced.

Based on the results of the unloaded race and the similar nature of the data on the thrust-loaded race, combined with the poorer data quality for the test cut, the effort was not made to process the data on the loaded race. Based on the data, it is clear that the same conclusion can be made: there are no significant residual stresses in the thrust-loaded race.

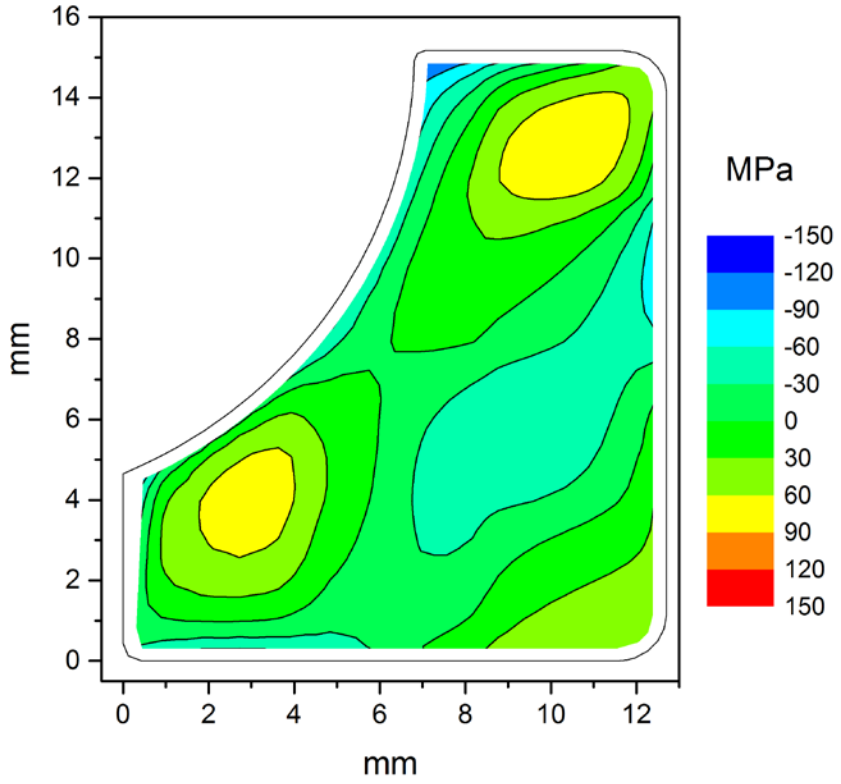

Figure 8. The measure residual stresses in the unloaded bearing race are mostly insignificant.

Upon further consideration, the lack of service-induced residual stress is less of a surprise. Subsurface residual stresses in bearings typically develop after a significant number of RCF cycles, from localized microplasticity, at elevated Hertzian stress. The small surface deformation and stress uncovered by the contour method thus implies that the hardened steel raceways of this bearing were not subjected to high Hertzian stresses or a substantially great amount of cycles. Because the bearing was conservatively removed from service prior to sufficient cycling loading, such stresses were not induced.

Conclusions and Future Plans

Contour method measurements showed no significant residual stresses in two races taken from a main-shaft roller bearing removed from service from an aircraft jet engine. The lack of stress in the race that did not see a thrust load indicates no residual stresses from the bearing manufacture, which is attributed primarily to the races being through-hardened as compared to case hardened. The lack of stress in the thrust-loaded counterpart race indicates that the in-service loading did not induce any new residual stresses. Since the precise in-service loading history of this race in not currently known, we cannot compare this result to expectations based on the details of the loading. However, the bearing was probably conservatively removed from service prior to sufficient cycling loading to induce stresses.

The data is encouraging for future measurements on races and other test parts where higher residual stresses are expected. The stress-free test cuts showed contours generally under ± 10 μm in amplitude, which should allow for reasonable resolution of stress-induced contours. Even more encouraging is that once the data was averaged between the two halves of a measurement cut and then corrected for the stress-free cut, see **Figure 7**, it shows even flatter data in the region near the curved bearing contact surface, which is the region of interest where we hope to resolve loading induced stresses in bearings

that have seen more significant loads. We should be able to resolve localized stresses in such a region if they exist.

This novel application of the contour method has paved the way and generated insights for future applications of the method on RCF components. Further investigations are anticipated using laboratory RCF-tested ball and rod specimens of both through and case-hardened bearing steels that have experienced a higher range of Hertzian stress and cycles.

ACKNOWLEDGEMENTS

The authors would like to thank Adrian DeWald and Hill Engineering, LLC for the expert experimental work, both EDM cutting and surface scanning, for the measurements reported in this paper. Gratitude is also expressed to Lewis Rosado, Kevin Thompson, Hitesh Trivedi and their colleagues in the Mechanical Systems Branch of the Air Force Research Laboratory for providing the bearing and their valuable support of the project thus far.

Los Alamos National Laboratory, an affirmative action/equal opportunity employer, is operated by the Los Alamos National Security, LLC for the National Nuclear Security Administration of the U.S. Department of Energy under contract DE-AC52-06NA25396. By approving this article, the publisher recognizes that the U.S. Government retains nonexclusive, royalty-free license to publish or reproduce the published form of this contribution, or to allow others to do so, for U.S. Government purposes. Los Alamos National Laboratory requests that the publisher identify this article as work performed under the auspices of the U.S. Department of Energy. Los Alamos National Laboratory strongly supports academic freedom and a researcher's right to publish; as an institution, however, the Laboratory does not endorse the viewpoint of a publication or guarantee its technical correctness.

REFERENCES

1. Withers PJ (2007) Residual stress and its role in failure. Reports on Progress in Physics 70 (12):2211-2264
2. James MN (2011) Residual stress influences on structural reliability. Engineering Failure Analysis 18 (8):1909-1920
3. Liu KK, Hill MR (2009) The effects of laser peening and shot peening on fretting fatigue in Ti-6Al-4V coupons. Tribology International 42 (9):1250-1262
4. Edwards L, Smith MC, Turski M, Fitzpatrick ME, Bouchard PJ (2008) Advances in residual stress modeling and measurement for the structural integrity assessment of welded thermal power plant. Advanced Materials Research 41-42:391-400
5. Aydiner CC, Ustundag E, Prime MB, Peker A (2003) Modeling and measurement of residual stresses in a bulk metallic glass plate. Journal of Non-Crystalline Solids 316 (1):82-95
6. Tanner DA, Robinson JS (2003) Modelling stress reduction techniques of cold compression and stretching in wrought aluminium alloy products. Finite Elements in Analysis and Design 39 (5/6):369-386
7. Yaghi AH, Hilson G, Simandjuntak S, Flewitt PEJ, Pavier MJ, Smith DJ, Hyde TH, Becker AA, Sun W (2010) A Comparison Between Measured and Modeled Residual Stresses in a Circumferentially Butt-Welded P91 Steel Pipe. Journal of Pressure Vessel Technology 132 (1):011206-011206. doi:10.1115/1.4000347
8. Rolph J, Preuss M, Iqbal N, Hofmann M, Nikov S, Hardy MC, Glavicic MG, Ramanathan R, Evans A (2012) Residual Stress Evolution during Manufacture of Aerospace Forgings. Huron ES, Reed RC, Hardy MC et al. (eds) Superalloys 2012. John Wiley & Sons, Inc., Hoboken, NJ, USA, pp 881-891. doi:10.1002/9781118516430.ch97
9. Dai H, Francis JA, Withers PJ (2010) Prediction of residual stress distributions for single weld beads deposited on to SA508 steel including phase transformation effects. Materials Science and Technology 26:940-949. doi:10.1179/026708309x12459430509454

10. DeWald AT, Hill MR (2009) Eigenstrain based model for prediction of laser peening residual stresses in arbitrary 3D bodies. Part 1: model description. Journal of Strain Analysis for Engineering Design 44 (1):1-11
11. Prime MB, Prantil VC, Rangaswamy P, Garcia FP (2000) Residual stress measurement and prediction in a hardened steel ring. Materials Science Forum 347-349:223-228
12. Muránsky O, Hamelin CJ, Smith MC, Bendeich PJ, Edwards L (2014) The Role of Plasticity Theory on the Predicted Residual Stress Field of Weld Structures. Materials Science Forum 772:65-71
13. Carlone P, Palazzo GS, Pasquino R (2010) Finite element analysis of the steel quenching process: Temperature field and solid–solid phase change. Computers & Mathematics with Applications 59 (1):585-594. doi:http://dx.doi.org/10.1016/j.camwa.2009.06.006
14. Tanner DA, Robinson JS (2000) Residual stress prediction and determination in 7010 aluminum alloy forgings. Experimental Mechanics 40 (1):75-82. doi:10.1007/bf02327551
15. Ismonov S, Daniewicz SR, Newman JJC, Hill MR, Urban MR (2009) Three Dimensional Finite Element Analysis of a Split-Sleeve Cold Expansion Process. Journal of Engineering Materials and Technology 131 (3):031007. doi:10.1115/1.3120392
16. Carlone P, Palazzo GS (2012) Experimental Analysis of the Influence of Process Parameters on Residual Stress in AA2024-T3 Friction Stir Welds. Key Engineering Materials 504-506:753-758. doi:10.4028/www.scientific.net/KEM.504-506.753
17. Kaiser R, Stefenelli M, Hatzenbichler T, Antretter T, Hofmann M, Keckes J, Buchmayr B (2015) Experimental characterization and modelling of triaxial residual stresses in straightened railway rails. The Journal of Strain Analysis for Engineering Design 50 (3):190-198. doi:10.1177/0309324714560040
18. Xie P, Zhao H, Wu B, Gong S (2015) Evaluation of Residual Stresses Relaxation by Post Weld Heat Treatment Using Contour Method and X-ray Diffraction Method. Experimental Mechanics 55 (7):1329-1337. doi:10.1007/s11340-015-0040-2
19. Zhang Z, Yang Y, Li L, Chen B, Tian H (2015) Assessment of residual stress of 7050-T7452 aluminum alloy forging using the contour method. Materials Science and Engineering: A 644:61-68. doi:http://dx.doi.org/10.1016/j.msea.2015.07.018
20. Vrancken B, Cain V, Knutsen R, Van Humbeeck J (2014) Residual stress via the contour method in compact tension specimens produced via selective laser melting. Scripta Materialia 87:29-32. doi:http://dx.doi.org/10.1016/j.scriptamat.2014.05.016
21. Sadeghi F, Jalalahmadi B, Slack TS, Raje N, Arakere NK (2009) A Review of Rolling Contact Fatigue. Journal of Tribology 131 (4):041403-041403. doi:10.1115/1.3209132
22. Voskamp AP, Österlund R, Becker PC, Vingsbo O (1980) Gradual changes in residual stress and microstructure during contact fatigue in ball bearings. Metals Technology 7 (1):14-21. doi:10.1179/030716980803286676
23. Österlund R, Vingsbo O Phase changes in fatigued ball bearings. Metallurgical Transactions A 11 (5):701-707. doi:10.1007/bf02661199
24. Voskamp AP (1985) Material Response to Rolling Contact Loading. Journal of Tribology 107 (3):359-364. doi:10.1115/1.3261078
25. Palmgren A (1959) Ball and roller bearing engineering. Philadelphia. SKF Industries Inc, Philadelphia
26. Lundberg G, Palmgren A (1947) Dynamic capacity of roller bearings. vol 196. Generalstabens litografiska anstalts förlag,
27. Lunberg G, Palmgren A (1952) 'Dynamic Capacity of Roller Bearings. Acta Polytech, Mech Eng Ser 2:96
28. Standard I, ISO B (2007) Rolling Bearing–Dynamic Load Ratings and Rating Life. ISO,
29. Zaretsky EV (1992) STLE life factors for rolling bearings. STLE SPECIAL PUBLICATION SP
30. Londhe ND, Arakere NK, Haftka RT (2015) Reevaluation of Rolling Element Bearing Load-Life Equation Based on Fatigue Endurance Data. Tribology Transactions 58 (5):815-828. doi:10.1080/10402004.2015.1021943
31. Voskamp AP, Mittemeijer EJ (1997) State of residual stress induced by cyclic rolling contact loading. Materials Science and Technology 13 (5):430-438. doi:10.1179/mst.1997.13.5.430
32. Schajer GS (2013) Practical residual stress measurement methods. John Wiley & Sons, Chichester,WestSussex, UK
33. Holden TM (2013) Neutron Diffraction. Schajer GS (ed) Practical Residual Stress Measurement Methods. John Wiley & Sons, Ltd, pp 195-223. doi:10.1002/9781118402832.ch8

34. Schajer GS, Whitehead PS (2013) Hole Drilling and Ring Coring. Schajer GS (ed) Practical Residual Stress Measurement Methods. John Wiley & Sons, Ltd, pp 29-64
35. Pagliaro P, Prime MB, Robinson JS, Clausen B, Swenson H, Steinzig M, Zuccarello B (2011) Measuring Inaccessible Residual Stresses Using Multiple Methods and Superposition. Experimental Mechanics 51 (7):1123-1134. doi:10.1007/s11340-010-9424-5
36. Prime MB, DeWald AT (2013) The Contour Method. Schajer GS (ed) Practical Residual Stress Measurement Methods. John Wiley & Sons, Ltd., Chichester,WestSussex, UK. doi:10.1002/9781118402832.ch5
37. Prime MB, Gonzales AR (2000) The Contour Method: Simple 2-D Mapping of Residual Stresses. The 6th International Conference on Residual Stresses, Oxford, U.K., 2000. IOM Communications, London, U.K., pp 617-624
38. Prime MB (2001) Cross-sectional mapping of residual stresses by measuring the surface contour after a cut. Journal of Engineering Materials and Technology 123 (2):162-168
39. Hill MR, Olson MD (2014) Repeatability of the Contour Method for Residual Stress Measurement. Experimental Mechanics 54 (7):1269-1277. doi:10.1007/s11340-014-9867-1
40. Toparli MB, Fitzpatrick M, Gungor S (2015) Determination of Multiple Near-Surface Residual Stress Components in Laser Peened Aluminum Alloy via the Contour Method. Metallurgical and Materials Transactions A 46 (9):4268-4275. doi:10.1007/s11661-015-3026-x
41. Woo W, An GB, Em VT, DeWald AT, Hill MR (2014) Through-thickness distributions of residual stresses in an 80 mm thick weld using neutron diffraction and contour method. Journal of Materials Science 50 (2):784-793
42. Braga DFO, Coules HE, Pirling T, Richter-Trummer V, Colegrove P, de Castro PMST (2013) Assessment of residual stress of welded structural steel plates with or without post weld rolling using the contour method and neutron diffraction. Journal of Materials Processing Technology 213 (12):2323-2328. doi:http://dx.doi.org/10.1016/j.jmatprotec.2013.07.004
43. Elmesalamy A, Francis JA, Li L (2014) A comparison of residual stresses in multi pass narrow gap laser welds and gas-tungsten arc welds in AISI 316L stainless steel. International Journal of Pressure Vessels and Piping 113:49-59. doi:http://dx.doi.org/10.1016/j.ijpvp.2013.11.002
44. Rolph J, Iqbal N, Hoffman M, Evans A, Hardy M, Glavicic M, Preuss M (2013) The effect of d0 reference value on a neutron diffraction study of residual stress in a γ/γ′ nickel-base superalloy. Journal of Strain Analysis for Engineering Design 48 (4):219-228. doi:10.1177/0309324713486273
45. Traore Y, Paddea S, Bouchard P, Gharghouri M (2013) Measurement of the Residual Stress Tensor in a Compact Tension Weld Specimen. Experimental Mechanics 53 (4):605-618. doi:10.1007/s11340-012-9672-7
46. Pagliaro P, Prime MB, Clausen B, Lovato ML, Zuccarello B (2009) Known Residual Stress Specimens Using Opposed Indentation. Journal of Engineering Materials and Technology 131:031002
47. Prime MB, DeWald AT, Hill MR, Clausen B, Tran M (2014) Forensic Determination of Residual Stresses and KI from Fracture Surface Mismatch. Engineering Fracture Mechanics 116:158-171. doi:10.1016/j.engfracmech.2013.12.008
48. Mahmoudi AH, Saei A (2015) Influence of asymmetrical cuts in measuring residual stresses using contour method. International Journal of Pressure Vessels and Piping 134:1-10. doi:http://dx.doi.org/10.1016/j.ijpvp.2015.08.004
49. Hosseinzadeh F, Bouchard P (2013) Mapping Multiple Components of the Residual Stress Tensor in a Large P91 Steel Pipe Girth Weld Using a Single Contour Cut. Experimental Mechanics 53 (2):171-181. doi:10.1007/s11340-012-9627-z
50. Olson MD, Hill MR (2015) A New Mechanical Method for Biaxial Residual Stress Mapping. Experimental Mechanics 55 (6):1139-1150. doi:10.1007/s11340-015-0013-5
51. Prime MB (2011) Contour Method Advanced Applications: Hoop Stresses in Cylinders and Discontinuities. Paper presented at the Engineering Applications of Residual Stress, Volume 8, doi:10.1007/978-1-4614-0225-1_2
52. Hosseinzadeh F, Kowal J, Bouchard PJ (2014) Towards good practice guidelines for the contour method of residual stress measurement. The Journal of Engineering
53. Johnson G (2008) Residual stress measurements using the contour method. Ph.D. Dissertation, University of Manchester. (Currently available at http://www.lanl.gov/contour),
54. Brown DW, Holden TM, Clausen B, Prime MB, Sisneros TA, Swenson H, Vaja J (2011) Critical Comparison of Two Independent Measurements of Residual Stress in an Electron-Beam Welded

Uranium Cylinder: Neutron Diffraction and the Contour Method. Acta Materialia 59 (3):864-873. doi:10.1016/j.actamat.2010.09.022
55. de Swardt RR (2003) Finite element simulation of crack compliance experiments to measure residual stresses in thick-walled cylinders. Journal of Pressure Vessel Technology 125 (3):305-308
56. Ahmad B, Fitzpatrick ME (2016) Minimization and Mitigation of Wire EDM Cutting Errors in the Application of the Contour Method of Residual Stress Measurement. Metallurgical and Materials Transactions A 47 (1):301-313. doi:10.1007/s11661-015-3231-7
57. Prime MB, Kastengren AL (2011) The Contour Method Cutting Assumption: Error Minimization and Correction. Proulx T (ed) Experimental and Applied Mechanics, Volume 6, vol 17. Conference Proceedings of the Society for Experimental Mechanics Series. Springer New York, pp 233-250. Currently available at http://www.lanl.gov/contour/. doi:10.1007/978-1-4419-9792-0_40
58. Prime MB, Sebring RJ, Edwards JM, Hughes DJ, Webster PJ (2004) Laser surface-contouring and spline data-smoothing for residual stress measurement. Experimental Mechanics 44 (2):176-184
59. Olson MD, DeWald AT, Prime MB, Hill MR (2015) Estimation of Uncertainty for Contour Method Residual Stress Measurements. Experimental Mechanics 55 (3):577-585. doi:10.1007/s11340-014-9971-2
60. Savaria V, Hoseini M, Bridier F, Bocher P, Arkinson P (2011) On the measurement of residual stress in induction hardened parts. Materials Science Forum 681:431-436